Stability of Future Low-Inertia Power Systems with Different Grid-forming Control Schemes

STABILITY OF FUTURE LOW-INERTIA POWER SYSTEMS WITH DIFFERENT GRID-FORMING CONTROL SCHEMES

Hannu Laaksonen

School of Technology and Innovations, University of Vaasa, Vaasa, Finland
hannu.laaksonen@uwasa.fi

Keywords: FREQUENCY STABILITY, INVERTER-BASED RESOURCES, GRID-FORMING, LOW-INERTIA, POWER SYSTEMS

Abstract

Different grid-forming and grid-following inverter control and synchronization schemes can affect and support the low-inertia power system frequency stability in different ways. It is of key importance, however, that frequency stability can be always secured with varying shares of grid-forming and grid-following inverters as well as rotating generators. This paper presents case studies with variable shares of two different type of grid-forming inverter-based resources, grid-following inverters and synchronous generators. Case studies are done with a simple power system modelled with PSCAD to study the effect of these resources on frequency stability after a load increase. In overall, paper presents multiple proposals to further improve frequency stability by enhanced control of the studied grid-forming inverters in the simulated cases.

1 Introduction

Existing inverter-based resources (IBRs) control and synchronization is based on grid-following (GFL) control which assumes that the power system frequency and voltage are controlled by traditional synchronous generators (SGs) with natural inertia. However, in the future the share of grid-forming (GFM) IBRs needs to be high enough to ensure frequency stability of the low-inertia power system during rapid changes in generation (due to weather-dependent renewables), consumption and network topologies. Grid-following GFL inverter is often described as a controlled current source with high parallel impedance and grid-forming GFM inverter as a voltage source with low series impedance. At the moment, however, there is no generally accepted definition for GFM control and multiple different proposals have been presented in the literature and pilots. [1]-[6]

In the future, short-term inertia estimation [7] of IBR-based power systems is expected to be increasingly needed in order to determine also the required amount of very fast frequency support from IBRs with varying share of GFLs and different type of GFMs. One way to provide this support is fast frequency response (FFR) markets. For example, GFL- or GFM-controlled battery energy storage system (BESS) can provide FFR service by its active power-frequency (*Pf*) -droop functionality. However, the delayed FFR or virtual inertia services of IBRs affected by the filtered frequency or rate-of-change of frequency (ROCOF) measurements have been one concern related to their utilization in low-inertia IBR-based power systems. Therefore, some recent grid code developments have also required SG or voltage source type of very fast active power support from large-scale transmission network-connected GFMs during disturbances in order to support the stability of the power system.

In the literature, different frequency control related services, like FFR, provision by BESSs is typically realized either by an individual large-scale BESS or by aggregating multiple small-scale BESSs. In addition to FFR service, BESSs can also provide other active (*P*) and reactive power (*Q*) related flexibility services which can be realized, for example, by various inverter local control modes or functions. These control schemes, like *Q* control, can also affect the stability of the GFM IBRs [8] and further to the stability of the corresponding power system with large amount of IBRs.

Synchronization of GFM and GFL IBRs is one main difference between them and has an effect also on their disturbance behavior and stability. GFL IBR is typically synchronized to measured or estimated grid voltage angle by phase-locked-loop (PLL) or frequency-locked-loop (FLL) component. On the other hand, most of the GFM IBR control schemes don't have a PLL or FLL. Instead, their synchronization can be based e.g. on droop or power synchronization. In the literature, different wide-area communication and time-synchronized measurements (e.g. from phasor measurement units, PMUs) based control schemes for future IBR-based power systems have also been proposed. For example, in [9]-[10] wide-synchronization control for GFM-based IBRs was presented and in [11] voltage angle control scheme has been proposed. On the other hand, also various online grid impedance estimation methods, e.g. [12] have been suggested to improve IBRs' stability in strong or weak grids.

In general, various IBR GFM and GFL control and synchronization schemes affect and support the power system frequency stability in different ways, but they should be

compatible with each other and adapt to varying system dynamics e.g. due to changes on the inertia level and network topology. Therefore, it is important that the power system frequency stability can be always kept and supported with varying shares of different GFM-based IBR control schemes, SGs and GFLs.

In the previous studies [13]-[16], universal FLL -based grid-forming and -supporting (U-FLL) synchronization method, which can directly replace the PLL-component of GFL inverters, has been proposed and simulated with multiple type of distributed energy resources (DERs). This paper presents case studies with PSCAD simulations in which the frequency stability and behavior of simple HV network model is studied with/without SG and with variable shares of two different type of GFM inverters i.e. GFM_A: U-FLL-based (multiple smaller IBRs) and GFM_B: multi-loop droop controlled [17] (one large IBR), SGs and GFL-inverters.

2. Simulation Study Cases

The main simulation study cases of this paper are summarised in Table 1. Fig. 1 shows the PSCAD simulation model of the used SG. The GFM_A BESS's average PSCAD model with controlled voltage sources and related control scheme with U-FLL based synchronization is presented in Fig. 2. The GFM_B IBR's multi-loop droop control scheme can be found from [17].

Table 1. Main study cases.

Case	Type and number of generating units	Synchronization of IBRs
CASE_HYBRID	***GFM_A***: BESS (2-18) ***GFM_B***: BESS (1) ***SG*** (1)	***GFM_A***: U-FLL ***GFM_B***: multi-loop droop [17]
CASE_IBR	***GFM_A***: BESS (4-68) ***GFM_B***: BESS (1)	

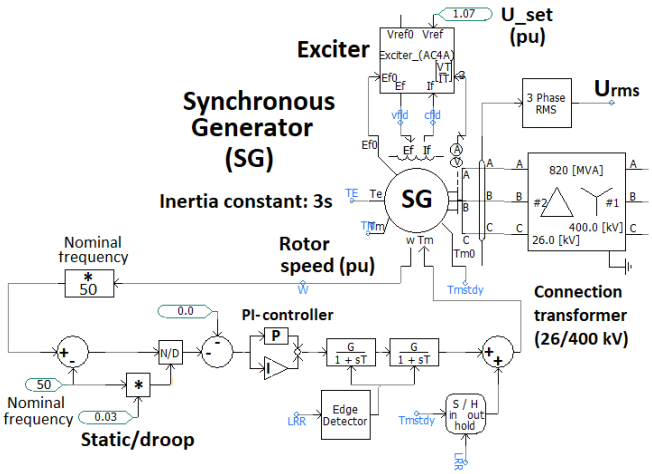

Fig. 1. HV network connected SG's PSCAD model.

In [13] it was stated that U-FLL and other GFM schemes should be also stable during long duration frequency deviations. In order to prevent loosing the stability of DER unit control if the U-FLL output phase angle deviates too much and/or too long from the actual voltage phase angle (e.g. followed by traditional PLL or U-FLL with constant correction coefficient 1, Fig. 2 and 3), for example, cumulative phase angle difference monitoring logic could be added in the U-FLL. Fig. 3 shows the enhanced U-FLL with phase angle difference monitoring which has been utilized in the PSCAD simulations of this paper.

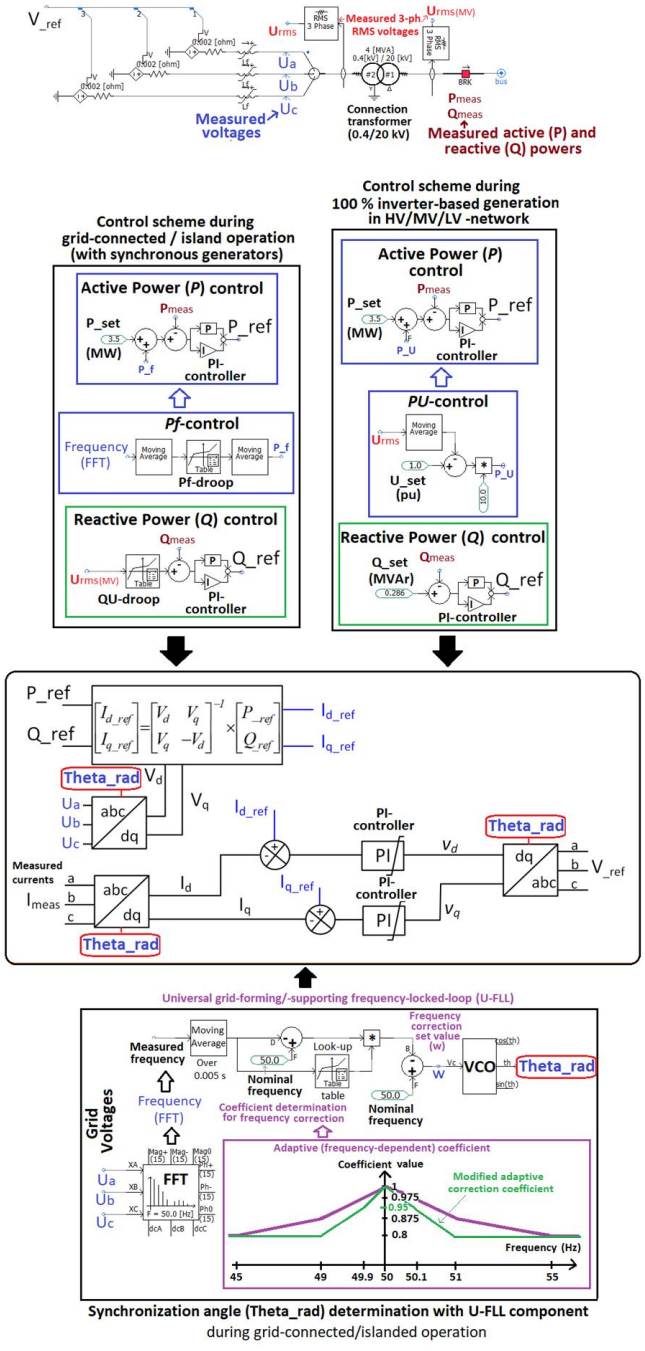

Fig. 2. GFM_A BESS's average PSCAD model with controlled voltage sources and related control scheme with U-FLL based synchronization.

In Fig. 4 and 5, the one-line diagrams of the main PSCAD simulation study cases (Table 1) CASE_HYBRID (Fig. 4) and CASE_IBR (Fig. 5) are presented.

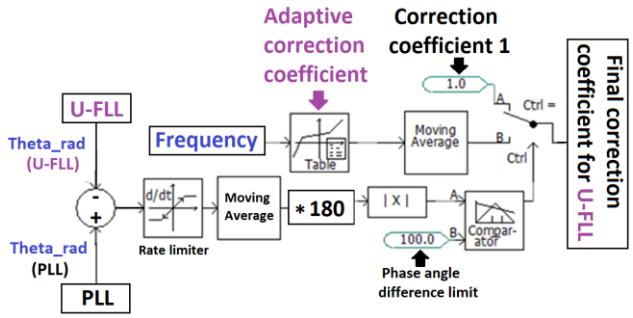

Fig. 3. Enhanced U-FLL with phase angle difference monitoring (GFM_A) based U-FLL correction coefficient.

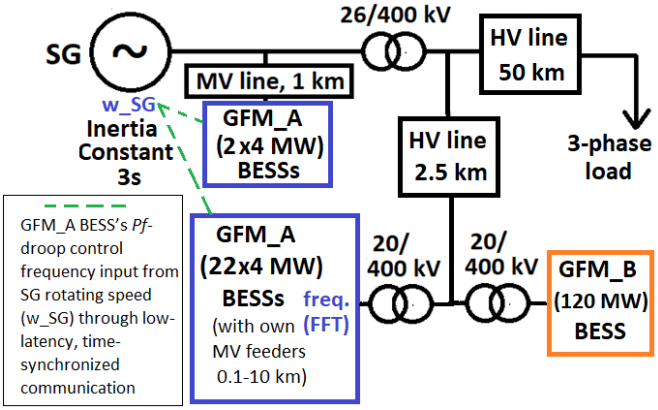

Fig. 4. One-line diagram of the hybrid small HV network (CASE_HYBRID, Table 1) with SG (Fig. 1), GFM_A BESSs (Fig. 2 and 3) and/or GFM_B [17].

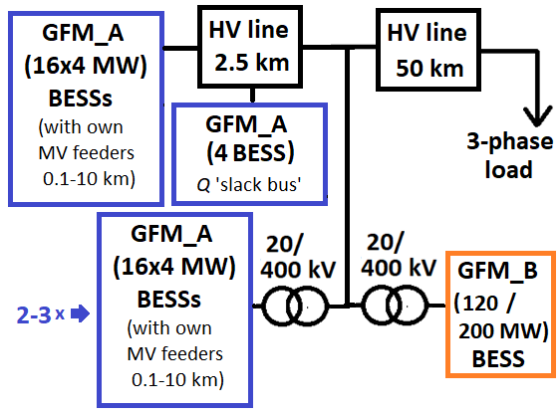

Fig. 5. One-line diagram of the 100 % IBR-based small HV network (CASE_IBR, Table 1) with GFM_A BESSs (Fig. 2 and 3) and/or GFM_B [17].

3 Simulation Results

In the following, main simulation results from the different study cases are presented. First, in Section 3.1 results from hybrid small HV power system (CASE_HYBRID, Table 1 & Fig. 4) are shown. After that, Section 3.2 presents the simulation results from the 100 % IBR-based small HV power system (CASE_IBR, Table 1 & Fig. 5).

3.1 Hybrid System with IBRs and SG

The total simulation time in the Section 3.1 subcases of the main study case CASE_HYBRID (Table 1) was t=20.0 s and 100 MW load increase at the end of 50 km transmission line (Fig. 4) happened at t=10.0 s. Before the load increase the total load was 505.5 MW in Section 3.1 subcases. Total active power generation of 22 (4 MW) GFM_A BESSs (Fig. 4) was 56 MW (11 % from the total load) and respectively P of one GFM_B BESS (Fig. 4) was 86 MW (17 % from the total load). With 22 GFM_A BESSs, the mode change from discharging to charging during frequency oscillations was disabled in the simulations of Section 3.1. Initial active power output of the two 4 MW GFM_A BESSs at the SG connection point (Fig. 4) was close to zero before the load increase and with these two GFM_A BESSs the mode change from discharging to charging during frequency oscillations was enabled.

3.1.1 Effect of Different GFM Control Schemes in Small Hybrid Power System with SG

The PSCAD simulation results from case CASE_HYBRID (Fig. 4 and Table 1) subcases (Table 2) for studying the effect of different GFM control schemes on frequency stability after the load increase at t=10.0 s are shown in Fig. 8.

Table 2. Study cases of Section 3.1.1 to study the effect of different GFM control schemes in small hybrid power system with SG (see also Table 1).

Subcase	Type and number & share (%) of IBR-based DER / SG	IBRs' active power *P* control
BASE CASE	- / SG (1 & 100 %)	-
CASE_HYBRID_GFM_B	***GFM_B*** (1 & **17 %**) / SG (1 & 83 %)	***GFM_B:*** Multi-loop droop, *P*-droop gain 0.05 [17]
CASE_HYBRID_GFM_A_1	***GFM_A*** (2 & **1.5 %**) / ***GFM_A*** (22 & **11 %**) / SG (1 & 87.5 %)	***GFM_A*** (2)*: Pf*-droop 1*) ***GFM_A*** (22): *Pf*-droop 1**)
CASE_HYBRID_GFM_A_2	***GFM_A*** (2 & **1.5 %**) / ***GFM_A*** (22 & **11 %**) / SG (1 & 87.5 %)	***GFM_A*** (2) & (22): *Pf*-droop 1*)
CASE_HYBRID_GFM_A_B	***GFM_A*** (2 & **1.5 %**) / ***GFM_B*** (1 & **17 %**) / SG (1 & 81.5 %)	***GFM_A*** (2)*: Pf*-droop 1*) ***GFM_B***: Multi-loop droop, *P*-droop gain 0.05 [17]

*) *Pf-control frequency input (Fig. 2) from SG speed with moving average over 5 ms (Fig. 7a),* **) *Pf-control frequency input (Fig. 2) from PSCAD FFT -block with moving average over 100+100 ms (Fig. 7b)*

When GFM_A BESS *Pf*-droop control input is directly from SG speed (Table 2), then moving average of *Pf*-control set value can be reduced to 5 ms (Fig. 7a) in order to improve the response speed of *Pf*-control with GFM_A. In some of the subcases shown in Table 2, the GFM_A *Pf*-control frequency

input comes either from SG speed with moving average over 5 ms (Fig. 7a and Table 2) or from PSCAD FFT -block with moving average over 100 ms before and after the *Pf*-droop (Fig. 7b and Table 2). Fig. 6 presents the GFM_A BESS's *Pf*-droop 1 which was utilized in the subcases of CASE_HYBRID (Table 2). GFM_B *P*-droop gain was 0.05 pu (Table 2). In Fig. 8, the measured frequencies, calculated from the rotating speed of SG (Fig. 1 and Fig. 4), after the load increase at *t*=10.0 s in CASE_HYBRID subcases (Table 2) are shown.

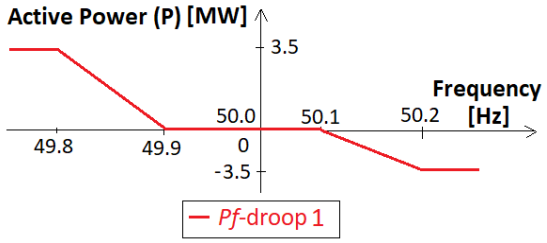

Fig. 6. GFM_A BESS's *Pf*-droop 1 settings (Fig. 2, Table 2).

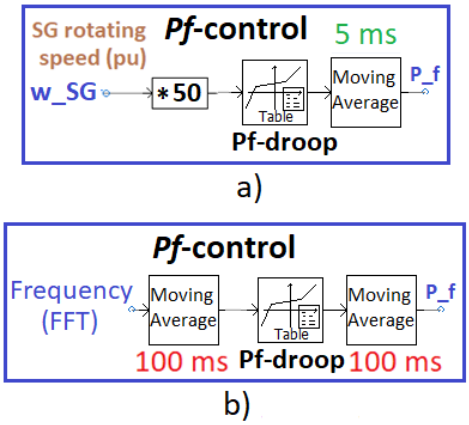

Fig. 7. GFM_A BESS's *Pf*-droop control frequency input filtering with moving averaging is a) 5 ms when frequency input comes from SG speed and b) 100 + 100 ms when frequency input comes from PSCAD FFT -block (Fig. 2, Table 2).

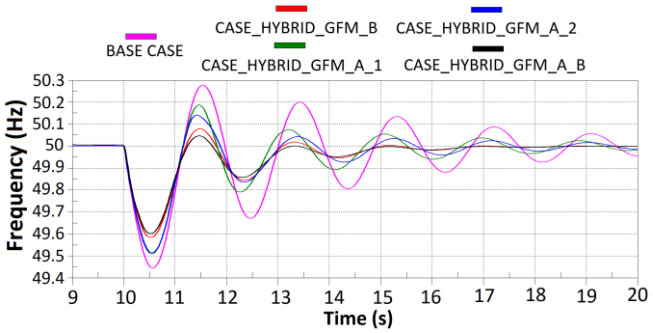

Fig. 8. Measured frequency calculated from rotor speed of SG after load increase at *t*=10.0 s with discharged GFM_A or GFM_B BESSs in CASE_HYBRID subcases (Table 2).

From Fig. 8 simulation results it can be seen that Table 2 subcases with GFM_B included (CASE_HYBRID_GFM_B, CASE_HYBRID_GFM_A_B) are the most stable ones from frequency stability viewpoint after the load increase at *t*=10.0 s. Smaller frequency stabilising effect of GFM_A subcases is partly due to the delayed active power response by the *Pf*-droop 1 (Fig. 6) with a dead zone between 49.9-50.1 Hz. However, when comparing subcases (CASE_HYBRID_GFM_A_1 and CASE_HYBRID_GFM_A_2) it can be seen that when the GFM_A BESSs' *Pf*-droop control (and U-FLL synchronization) frequency input comes from SG rotating speed (Table 2, Fig. 4), the frequency stability can be improved.

3.1.2 Effect of Enhanced GFM Control Schemes in Small Hybrid Power System with SG

The PSCAD simulation results from CASE_HYBRID (Fig. 4 and Table 1) subcases (Table 3) for studying the effect of enhanced GFM control schemes on frequency stability after the load increase at *t*=10.0 s are shown in Fig. 11-13. GFM_A *Pf*-control frequency input comes either from SG speed with moving average over 5 ms (Fig. 7a and Table 3) or from PSCAD FFT -block with rate limiter (Fig. 10) and moving average over 75 ms before and after the *Pf*-droop (Fig. 10 and Table 2). Fig. 9 presents the GFM_A BESS's more sensitive *Pf*-droop 2 that were used in Table 3 subcases. With *Pf*-droop 2 (Fig. 9, Table 3) large part of the active power capacity is reserved constantly for the rapid *Pf*-control purposes in order to provide better frequency stability support from the GFM_A BESSs. GFM_B *P*-droop gain was also changed to 0.03 pu (Table 3). In Fig. 11, the measured frequencies, calculated from the rotating speed of SG (Fig. 1 and Fig. 4), after the load increase at *t*=10.0 s in CASE_HYBRID subcases (Table 3) are shown. Fig. 12 presents the total active power of GFM_A BESSs (22) / GFM_B BESS (1) in different cases (Table 3). HV transmission line voltages at the end of the line (close to 3-phase load, Fig. 4) are shown in Fig. 13.

Table 3. Study cases of Section 3.1.2 to study the effect of enhanced GFM control schemes in small hybrid power system with SG (see also Tables 1 & 2).

Subcase	Type and number & share (%) of IBR-based DER / SG	IBRs' active power *P* control
CASE_HYBRID_GFM_B_2	***GFM_B*** (1 & **17 %**) / SG (1 & 83 %)	***GFM_B:*** Multi-loop droop, *P*-droop gain 0.03 [17]
CASE_HYBRID_GFM_A_3	***GFM_A*** (2 & **1.5 %**) / ***GFM_A*** (22 & **11 %**) / SG (1 & 87.5 %)	***GFM_A*** (2)*:* *Pf*-droop 2*) ***GFM_A*** (22): *Pf*-droop 2 **)
CASE_HYBRID_GFM_A_4	***GFM_A*** (2 & **1.5 %**) / ***GFM_A*** (22 & **11 %**) / SG (1 & 87.5 %)	***GFM_A*** (2) & (22): *Pf*-droop 2*)

*) *Pf-control frequency input (Fig. 2) from SG speed with moving average over 5 ms (Fig. 7a),* **) *Pf-control frequency input (Fig. 2) from PSCAD FFT -block with rate limiter and moving average over 75+75 ms (Fig. 10)*

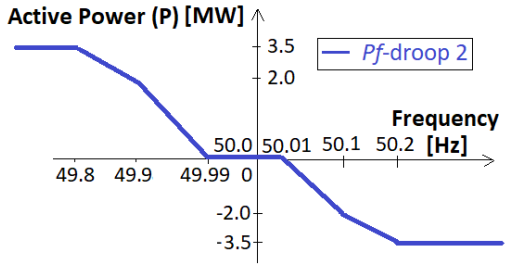

Fig. 9. GFM_A BESS's *Pf*-droop 2 settings (Fig. 2, Table 3).

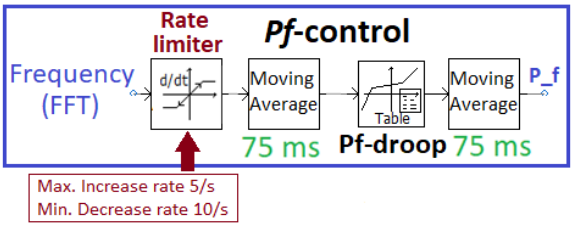

Fig. 10. GFM_A BESS's *Pf*-droop control frequency input filtering with rate limiter and moving averaging is 75 + 75 ms when frequency input comes from PSCAD FFT -block (Fig. 2, Table 3).

From Fig. 11 simulation results it can be seen that Table 3 subcases CASE_HYBRID_GFM_B_2 with GFM_B having *P*-droop gain 0.03 can further improve the frequency stability from the Section 3.1.1 results (Fig. 8). However, the use of more sensitive *Pf*-droop 2 (Fig. 9) on GFM_A BESSs significantly improves their performance (Fig. 11). In addition, in CASE_HYBRID_GFM_A_4 with *Pf*-droop control and U-FLL synchronization input coming from SG rotating speed (Table 3, Fig. 4) the frequency can be stabilised even more rapidly after the first frequency swing than in the case with enhanced GFM_B (CASE_HYBRID_GFM_B_2). On the other hand, use of SG speed as the input frequency requires time-synchronized (e.g. IEEE 1588 PTP-based) low-latency wireless communication (5G/6G) and also local frequency measurement (like in Fig. 10) as a back-up. When comparing the results (Fig. 11-13), it should be also noted that the relative share of GFM_B is higher than GFM_A(s) and it can partly also affect the results.

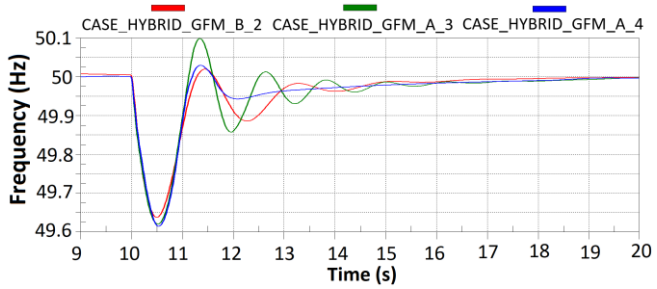

Fig. 11. Measured frequency calculated from rotor speed of SG after load increase at *t*=10.0 s with discharged GFM_A BESSs (22) / GFM_B BESS (1) in CASE_HYBRID subcases (Table 3).

Fig. 12 shows the total active power of GFM_A BESSs (22) / GFM_B BESS (1) after the load increase at *t*=10.0 s in Table 3 subcases. It can be seen from Fig. 12 that the active power *P* of GFM_B rapidly decreases after the first rapid increase (i.e. oscillates after the load change) in CASE_HYBRID_GFM_B_2. However, the *P* of GFM_A(s) in CASE_HYBRID_GFM_A_4 is much more stable, directly dependent on the frequency behaviour and therefore easy to forecast and estimate.

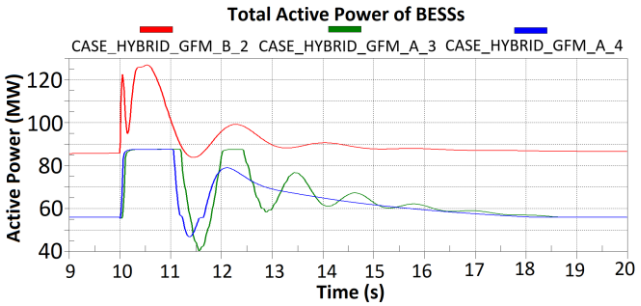

Fig. 12. Total active power of GFM_A BESSs (22) / GFM_B BESS (1) after load increase at *t*=10.0 s in CASE_HYBRID subcases (Table 3).

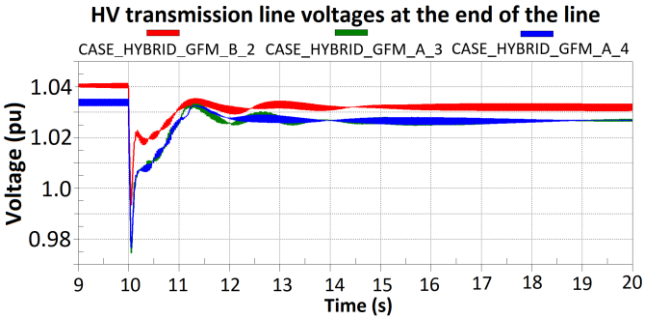

Fig. 13. HV transmission line voltages at the end of the line (close to 3-phase load, Fig. 4) after load increase at *t*=10.0 s in CASE_HYBRID subcases. (Table 3).

In overall, it can be stated that the enhanced schemes with GFM_A in Table 3 seemed to be very promising from the power system frequency stability support viewpoint. On the other hand, local frequency-based measurement e.g. as in Fig. 10 could be also used in demand response, frequency-dependent OLTC operation [18]-[21] and under-frequency-load-shedding (UFLS) in order to improve their response speed and frequency stability support.

3.2 100 % IBR-based System

In this Section 3.2, the simulation results with 100 % IBR-based generation in the main study case CASE_IBR (Table 1, Fig. 5) subcases are shown. It was concluded in [13] that the U-FLL-based synchronization can enable stable frequency, also after load increase, in 100 % IBR-based small HV network with GFM_A BESSs connected in MV network many kilometers away from each other (each GFM_A BESS had their own 0.1-10 km long MV feeder and 0.4/20 kV connection transformer, Fig. 5). Each of the 48-64 GFM_A BESSs (total number dependent on the subcase) produced 3.5 MW active power and the *P* of each 4 GFM_A 'slack bus' BESSs' was 1.5 MW (Fig. 5). These 4 BESSs also acted as reactive power "slack bus" during 100 % IBR operation i.e.

reactive power Q reference input was 0. In a power system with 100 % GFM_A-based DER units the *Pf*-control was not feasible [13] and therefore *PU*-control and *Q*-control were used with BESSs (Fig. 2). However, GFM_A IBRs' *Pf*-droop control (Fig. 14) was also added together with *PU*-control in two subcases of this Section 3.2, with only GFM_A BESSs and with GFM_A and GFM_B BESSs, in order to see *Pf*-control's effect on the frequency stability. In this Section 3.2 the total load at the end of 50 HV transmission line was 225 MW. During the 30.0 s simulation load increased 15 MW at the end of 50 km HV transmission line at t=15.0 s.

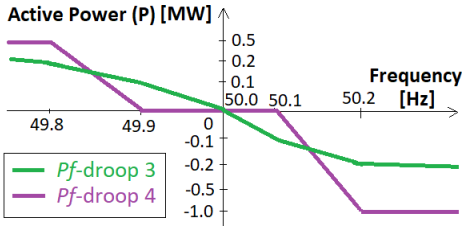

Fig. 14. GFM_A BESS's *Pf*-droop 3 and 4 settings (Fig. 2, Tables 4 and 6).

3.2.1 Effect of Different GFM_A & GFL Shares and Control Schemes in IBR-based System

The simulation results from CASE_IBR (Fig. 5 and Table 1) subcases (Table 4) for studying the effect of different GFM_A & GFL shares and control schemes on frequency stability after the load increase at t=15.0 s are shown in Fig. 15 and effect on HV line voltages are presented in Fig. 16.

Table 4. Study cases of Section 3.2.1 to study the effect of different GFM_A & GFL shares and control schemes in small 100% IBR-based power system (see also Table 1).

Subcase	Type and share (%) of IBR-based DER	IBRs' *P*- and *Q*-power control
CASE_IBR_GFM_A	***GFM_A* (100 %)**	***GFM_A***: *PU*- and *Q*-control
CASE_IBR_GFM_A_Pf	***GFM_A* (100 %)**	***GFM_A***: *Pf*-droop 3, *PU*- and *Q*-control
CASE_IBR_GFM_A_2	***GFM_A* (50 %)** ***GFL* (50 %)**	***GFM_A***: *PU*- and *Q*-control ***GFL***: *PU*- and *Q*-control
CASE_IBR_GFM_A_3	***GFM_A* (15 %)** ***GFL* (85 %)**[*)]	
CASE_IBR_GFM_A_4[**)]		
CASE_IBR_GFM_A_5[**),o)]		

*) *U-FLL-based synchronization with correction coefficient 1 (Fig. 2),* **) *GFM_A with modified adaptive correction coefficient (Fig. 2),* o) *GFLs at the end of HV line (close to 3-phase load) (Fig. 5)*

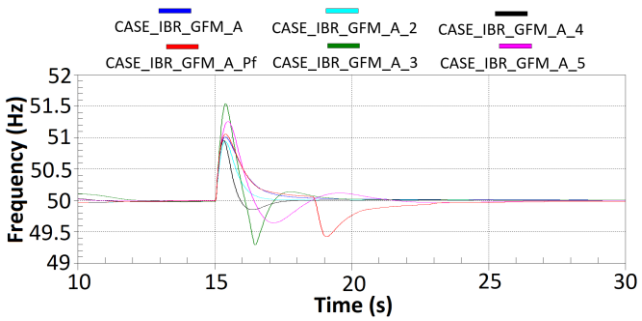

Fig. 15. Frequency after load increase at t=15.0 s in Table 4 subcases.

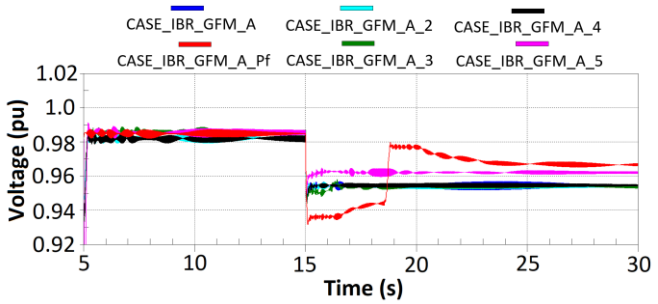

Fig. 16. HV transmission line voltages at the beginning of the line (Fig. 5) after load increase at t=15.0 s in CASE_IBR subcases (Table 4).

From Fig. 15 and 16 it can be seen that the *Pf*-control (CASE_IBR_GFM_A_Pf) with 100 % GFM_A has the largest frequency and voltage oscillations and does not provide any added value to the stability. Interestingly the Fig. 15 shows also that the frequency stability can be also well maintained in the other Table 4 cases with lower share (i.e. 50 % or 15 %) of GFM_A IBRs.

3.2.2 Effect of Different GFM_A & GFM_B Control Schemes and Shares in IBR-based System

The PSCAD simulation results from CASE_IBR (Fig. 5 and Table 1) subcases (Table 5) for studying the effect of different GFM_A & GFM_B shares and control schemes on frequency stability after the load increase at t=15.0 s are shown in Fig. 17.

Table 5. Study cases of Section 3.2.2 to study the effect of different GFM_A & GFM_B shares and control schemes in small 100% IBR-based power system (see also Table 1).

Subcase	Type and share (%) of IBR-based DER	IBRs' *P*- and *Q*-power control
CASE_IBR_GFM_AB	***GFM_A* (10 %)** ***GFM_B* (90 %)**	***GFM_A***: *PU*- and *Q*-control ***GFM_B:*** Multi-loop droop, *P*-droop gain 0.05 [17]
CASE_IBR_GFM_AB_2	***GFM_A* (62 %)** ***GFM_B* (38 %)**	
CASE_IBR_GFM_AB_3[o)]	***GFM_A* (62 %)** ***GFM_B* (38 %)**	

o) *GFM_B at the end of HV line (close to 3-phase load) (Fig. 5)*

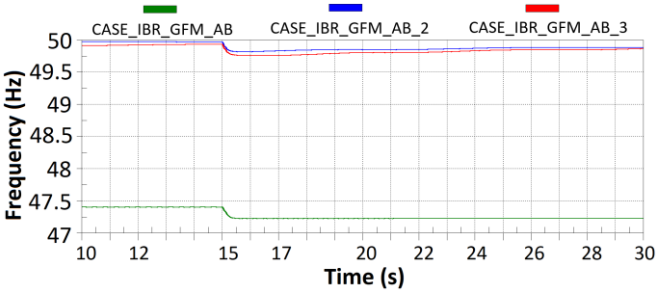

Fig. 17. Frequency after load increase at t=15.0 s in Table 5 subcases.

Fig. 17 illustrates that with 90 % share of GFM_B and 10 % of GFM_A (CASE_IBR_GFM_AB), the steady-state frequency is very low (< 47.5 Hz). However, when share of GFM_A is 62 % and GFM_B 38 % (Table 5, Fig. 17) then

the steady-state frequency and frequency level after load increase at *t*=15.0 s remains above 49.75 Hz.

3.2.3 Effect of Different GFM_A & GFM_B & GFL Control Schemes and Shares in IBR-based System

The simulation results from CASE_IBR (Fig. 5 and Table 1) subcases (Table 6) for studying the effect of different GFM_A & GFM_B & GFL shares and control schemes on frequency stability after the load increase at *t*=15.0 s are shown in Fig. 18.

Table 6. Study cases of Section 3.2.3 to study the effect of different GFM_A & GFM_B & GFL shares and control schemes in small 100% IBR-based power system (see also Table 1).

Subcase	Type and share (%) of IBR-based DER	IBRs' *P*- and *Q*-power control
CASE_IBR_GFM_B	***GFM_B* (38 %)** ***GFL* (62 %)**[*)]	***GFM_B:*** Multi-loop droop, *P*-droop gain 0.05 [17] ***GFL***: *PU*- and *Q*-control
CASE_IBR_GFM_AB_4[o)]	***GFM_A* (62 %)** ***GFM_B* (38 %)**	***GFM_A***: *PU*- and *Q*-control ***GFM_B:*** Multi-loop droop, *P*-droop gain 0.05 [17]
CASE_IBR_GFM_AB_4_Pf[o)]		***GFM_A***: *Pf*-droop 4, *PU*- and *Q*-control ***GFM_B:*** Multi-loop droop, *P*-droop gain 0.05 [17]
CASE_IBR_GFM_AB_5	***GFM_A* (31 %)** ***GFM_B* (38 %)** ***GFL* (31 %)**[*)]	***GFM_A***: *PU*- and *Q*-control ***GFM_B:*** Multi-loop droop, *P*-droop gain 0.05 [17] ***GFL***: *PU*- and *Q*-control
CASE_IBR_GFM_AB_6[**)]		

[*)] U-FLL-based synchronization with correction coefficient 1 (Fig. 2), [**)] GFM_A with modified adaptive correction coefficient (Fig. 2), [o)] GFM_A with U-FLL phase angle difference limit 150 ° (Fig. 3)

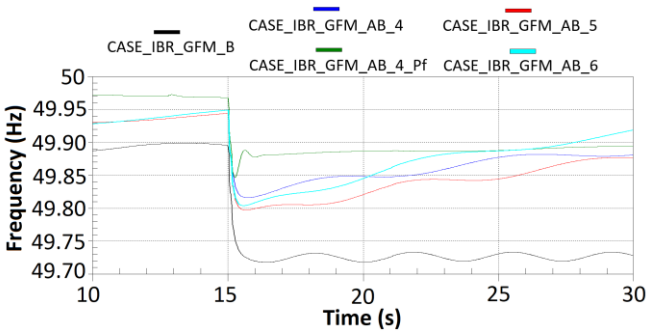

Fig. 18. Frequency after load increase at *t*=15.0 s in Table 6 subcases.

Fig. 18 shows that with 38 % share of GFM_B and 62 % of GFL (CASE_IBR_GFM_B), the frequency level after load increase at *t*=15.0 s is the lowest (above 49.7 Hz) from Table 6 subcases. Based on Fig. 17 and 18 it seems that very high share of GFM_B leads to lower steady-stage frequency levels. On the other hand, from Fig. 18 one can see that different enhancements of GFM_A IBRs control scheme in other Table 6 subcases can enable frequency level restoration after the load increase.

4 Conclusions

In the future low-inertia power systems the share of GFM IBRs must be sufficient to ensure frequency stability during rapid changes. Different IBR GFM and GFL control and synchronization schemes affect and can support the power system frequency level and stability in different ways. However, all schemes should be compatible with each other and adapt to varying system dynamics. It is of key importance that the frequency stability can be always kept with varying shares of different GFMs, SGs and GFLs.

This paper presented case studies in which the frequency stability and behaviour of simple HV network model was studied with and without SG as well as with variable share of two different type of GFMs (U-FLL-based GFM_A and multi-loop droop-based GFM_B), SGs and GFLs. In addition, U-FLL stability enhancing phase angle difference monitoring logic was presented (Fig. 3) and used in the simulations. Based on the PSCAD simulations of this paper following conclusions were made:

<u>Small hybrid power system with IBRs and SG</u>

- GFM_B with smaller *P*-droop gain supported the small hybrid power system frequency stability well
- Use of more sensitive *Pf*-droop 2 on GFM_A BESSs improved their performance
- Local frequency-based measurement (Fig. 10) used with GFM_A BESSs *Pf*-droop control improved their response and frequency stability support
- When the GFM_A BESSs' *Pf*-droop control and U-FLL synchronization input comes from SG rotating speed, the frequency stability could be even further improved
- With GFM_A more sensitive *Pf*-droop 2 and U-FLL synchronization input frequency coming from SG rotating speed, frequency could be stabilised even more rapidly after the first frequency swing than with GFM_B
- The active power *P* of GFM_B rapidly decreased after the first rapid increase (i.e. oscillated after the load change), *P* of GFM_A was much more stable and directly dependent on the frequency

<u>Small 100 % IBR-based power system</u>

- *Pf*-control with 100 % GFM_A did not provide any added value to the small power system frequency stability
- Frequency stability could be also well maintained with lower share of (i.e. 50 % or 15 %) GFM_A IBRs (without GFM_B IBRs
- Very high share of GFM_B (when compared to GFM_A and GFL) led to lower steady-stage frequency levels
- Different simulated/proposed modifications of GFM_A IBRs control scheme could enable frequency level restoration after the load increase in a system with varying share of GFM_B, GFM_A and GFL IBRs

In the future, more fast frequency support during normal operation and disturbances will be needed from IBRs in order to secure the frequency stability of the low-inertia power systems. This may require also creation of new markets for very fast frequency support or modification of the existing markets. On the other hand, with 100 % IBR-based power system traditional frequency reserve markets may not be feasible anymore (depending on the control and synchronization schemes of the IBRs). Possibly future active and reactive power related flexibility service markets could be more adaptive and collaborative with different levels, operation principles and response speed requirements depending on the short-term needs of the TSO and DSOs. In the future, it should be carefully considered also that what kind of grid-forming / -supporting functionality is required from MV and LV distribution network-connected IBRs. Future-proof functionality should be compatible with the distribution network operation, control, protection (including islanding detection) and market schemes with increased TSO-DSO coordination and collaboration. In the previous studies as well as in this paper, the U-FLL -based grid-forming and -supporting synchronization method together with the studied enhanced *Pf*-droop schemes based on different frequency inputs and their processing/filtering methods have shown potential and general applicability to be used with different size of IBRs connected at different voltage levels together with other GFMs, GFLs and SGs.

5 Acknowledgements

This work has been done as a part of “Smart Grid 2.0” -project funded by Business Finland with grant No. 1386/31/2022.

6 References

[1] Shrestha, A., Gonzalez-Longatt, F.: 'Frequency Stability Issues and Research Opportunities in Converter Dominated Power System', Energies, 2021, 14, 4184

[2] Mohammed, N., Alhelou, H. H., Bahrani, B.: 'Grid-Forming Power Inverters - Control and Applications' (CRC Press, 2023, 1st Edition)

[3] Rathnayake, D. B. et al., 'Grid Forming Inverter Modeling, Control, and Applications', IEEE Access, 2021, 9, pp. 114781-114807

[4] Musca, R., Gonzalez-Longatt, F., Gallego Sánchez, C.A.: 'Power System Oscillations with Different Prevalence of Grid-Following and Grid-Forming Converters', Energies, 2022, 15, 4273

[5] Musca, R., Vasile, A., Zizzo, G.: 'Grid-forming converters. A critical review of pilot projects and demonstrators', Renewable and Sustainable Energy Reviews, 2022, 165

[6] Marchand, J., Buire, J., Debusschere, V., Jarrai, N. E., Pompée J., Hadjsaid, N.: 'Large-Signal Stability of Inverter-Based LV Microgrids: Share of Grid-Forming Units', Proc. IEEE PES Innovative Smart Grid Technologies Europe (ISGT EUROPE), Grenoble, France, 2023

[7] Riquelme-Dominguez, J. M., Carranza-García, M., Lara-Benítez, P., González-Longatt, F.: 'A machine learning-based methodology for short-term kinetic energy forecasting with real-time application: Nordic Power System case', International Journal of Electrical Power & Energy Systems, 2024, 156

[8] Mohammed, N., Zhou W., Bahrani, B.: 'Impacts of the Reactive Power Control on the Small-signal Stability of Grid Forming Inverters', Proc. ISGT Asia, Auckland, New Zealand, 2023

[9] Musca, R., Sanseverino, E. R., Zizzo, G., Giannuzzi G., Pisani, C.: 'Wide-Synchronization Control for Power Systems with Grid-Forming Converters', IEEE Transactions on Power Systems, 2023

[10] Musca, R., Just, H.: 'Damping-enhanced schemes and wide-synchronization control for grid-forming converters', Proc. 22nd Wind and Solar Integration Workshop (WIW 2023), Copenhagen, Denmark, 2023

[11] Alhomsi, H., F. Linke, F., Westermann, D.: 'Concept of a new three-stage power system operation regime based on voltage angle control', Proc. IEEE PES Innovative Smart Grid Technologies Europe (ISGT EUROPE), Grenoble, France, 2023

[12] Mohammed, N., Ravanji, M. H., Zhou W., Bahrani, B.: 'Online Grid Impedance Estimation-Based Adaptive Control of Virtual Synchronous Generators Considering Strong and Weak Grid Conditions', IEEE Transactions on Sustainable Energy, 2023, 14, 1

[13] Laaksonen, H.: 'Universal Grid-forming Method for Future Power Systems', IEEE Access, 2022

[14] Laaksonen, H.: 'Improvement of Power System Frequency Stability with Universal Grid-forming Battery Energy Storages', IEEE Access, 2023

[15] Laaksonen, H.: 'Solutions to Improve Transient Stability of Universal Grid-forming Inverter-based Resources', Int. Review of Electrical Engineering (IREE), 2023, 18, 3

[16] Laaksonen, H.: 'Islanding Detection with Universal Grid-forming Inverter-based Generation', Proc. CIRED 2023, Rome, Italy, 2023

[17] Kenyon, R. W., Sajadi, A., Hoke, A., Hodge, B.-M.: 'Open-Source PSCAD Grid-Following and Grid-Forming Inverters and A Benchmark for Zero-Inertia Power System Simulations', Proc. IEEE Kansas Power and Energy Conference (KPEC), Manhattan, KS, USA, 2021

[18] Laaksonen, H., Khajeh, H., Parthasarathy, C., Shafie-khah, M., Hatziargyriou, N.: 'Towards Flexible Distribution Systems: Future Adaptive Management Schemes', Applied Sciences, 2021, 11, 8, 3709

[19] Laaksonen, H., Parthasarathy, C., Khajeh, H., Shafie-khah, M., Hatziargyriou, N.: 'Flexibility Services Provision by Frequency-Dependent Control of On-Load Tap-Changer and Distributed Energy Resources', IEEE Access, 2021, 9

[20] Laaksonen, H., Khajeh, H., Hatziargyriou, N.: 'Novel DER and OLTC Management Scheme for Coordinated TSO-DSO Flexibility Services Provision', Proc. IEEE PES ISGT Europe 2023, Grenoble, France, 2023

[21] Laaksonen, H., Khajeh, H., Hatziargyriou, N.: 'Coordinated Control Schemes for Improved DER Hosting Capacity and Flexibility Provision', Proc. CIRED 2024 Workshop on Increasing Distribution Network Hosting Capacity, Vienna, Austria, 2024